Broadband Nonreciprocal Thermal Emission

Zhenong Zhang and Linxiao Zhu*

Department of Mechanical Engineering, The Pennsylvania State University, University Park, Pennsylvania 16802, USA

(Received 7 July 2022; revised 10 October 2022; accepted 6 December 2022; published 5 January 2023)

The reciprocity between thermal emission and absorption in materials that satisfy the Lorentz reciprocity places a fundamental constraint on photonic energy conversion and thermal management. For approaching the ultimate thermodynamic limits in various photonic energy conversions and achieving nonreciprocal radiative thermal management, broadband nonreciprocal thermal emission is desired. However, existing designs of nonreciprocal emitters are narrowband. Here, we introduce a gradient epsilon-near-zero magneto-optical metamaterial for achieving broadband nonreciprocal thermal emission. We start by analyzing the nonreciprocal thermal emission and absorption in a thin layer of epsilon-near-zero magneto-optical material atop a substrate. We use temporal coupled-mode theory to elucidate the mechanism of nonreciprocal emission in the thin-film emitter. We then introduce a general approach for achieving broadband nonreciprocal emission by using a gradient epsilon-near-zero magneto-optical metamaterial. We numerically demonstrate broadband nonreciprocal emission in gradient-doped semiconductor multilayer, as well as in a magnetic Weyl semimetal multilayer with gradient chemical potential. Our approach for achieving broadband nonreciprocal emitters is useful for developing broadband nonreciprocal devices for energy conversion and thermal management.

DOI: 10.1103/PhysRevApplied.19.014013

I. INTRODUCTION

Controlling thermal emission and absorption is important for applications [1–4] in energy conversion, thermal management, lighting, and imaging. Various photonic structures and materials are used to control emission and absorption, such as metamaterials [5,6], metasurfaces [7,8], photonic crystals [9–11], multilayer [12,13], epsilon-near-zero materials [14,15], two-dimensional materials [16,17], and phase-change materials [18], leading to applications such as thermophotovoltaics [19–21], solar cells [22,23], and radiative cooling [12,24]. However, emission and absorption processes are typically constrained by a reciprocity relationship. The Kirchhoff's law of thermal radiation [25–27] states that emissivity equals absorptivity at the same angle and frequency. Such reciprocity between emission and absorption places a stringent constraint on the performance of a range of applications, such as solar cells [28–30], thermophotovoltaics [31], and harvesting outgoing radiation [31,32].

Achieving nonreciprocal emission and absorption points to a fundamental pathway for improving a range of energy-harvesting technologies, such as solar energy harvesting [28–30], thermophotovoltaics [31], harvesting energy from outgoing radiation [31], and simultaneously harvesting energy from the sun and outer space [32]. Importantly, to achieve the ultimate thermodynamic limits in these applications [28–32], nonreciprocal emission and absorption both need be achieved over a broad band. A reciprocal solar cell needs to emit luminescence towards the sun. Such luminescence cannot be used, and it represents energy loss. In contrast, a nonreciprocal solar cell can emit luminescence towards a direction away from the sun. Such luminescence can be collected using additional solar cells, leading to improvement of the overall efficiency. It is pointed out that, by using an array of nonreciprocal multijunction solar cells [29] or a nonreciprocal semitransparent multijunction solar cell [30], which achieve nonreciprocal emission over all wavelengths, the efficiency can approach the Landsberg limit of 93.3%. Such efficiency is substantially higher than the limit of 86.8% in reciprocal systems. For thermophotovoltaics, the use of nonreciprocal emitters points to the possibility of achieving the Carnot efficiency limit with maximum power output, which is impossible with reciprocal systems [31]. We also note that, by using narrowband nonreciprocal emitters in thermophotovoltaics, it is possible to achieve the Carnot efficiency limit, but with reduced power output. Furthermore, broadband nonreciprocal emitters point to the great potential for improving harvesting energy from outgoing thermal radiation. For harvesting thermal radiation from an ambient atmosphere at 300 K to outer space at 3 K, with nonreciprocal systems, the operating power density can approach the Landsberg limit [31] at 153.1 $\mathrm{W\,m^{-2}}$, which greatly

*lqz5242@psu.edu

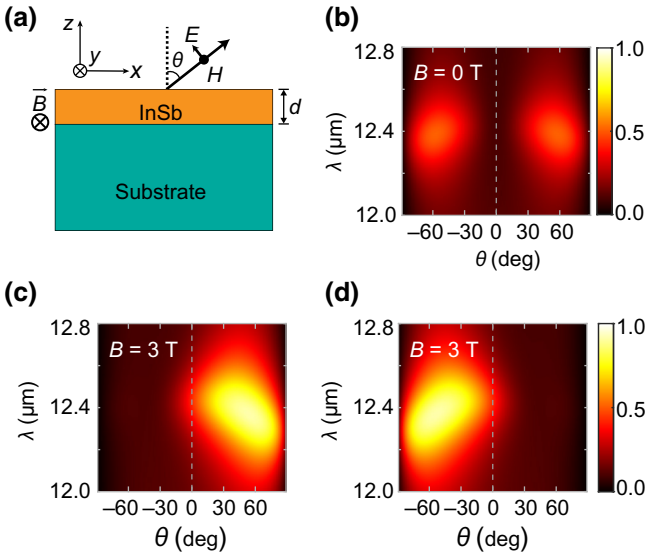

FIG. 1. Nonreciprocal emitter based on one layer of magneto-optical material. (a) Schematic of a doped InSb layer on top of a substrate. InSb layer has a thickness of 400 nm and is doped with an electron concentration of 8×10^{18} cm^{-3}. Substrate has constant relative permittivity $\epsilon_S = -2$. (b) Calculated emissivity, ε, and absorptivity, α, of the structure in (a) as a function of wavelength and angle when there is no external magnetic field. Here, emissivity and absorptivity are identical. (c) Calculated emissivity, ε, and (d) absorptivity, α, of the structure in (a) under a 3-T magnetic field. Emissivities in (b),(c) are calculated using fluctuational electrodynamics.

exceeds the limit of 55 W m^{-2} in reciprocal systems [31]. Also, broadband nonreciprocal emitters point to improving coharvesting energy from the sun and outer space [32].

Besides energy harvesting, achieving nonreciprocal emission and absorption points to nonreciprocal heat-flux control [33] and communication [34]. For nonreciprocal heat-flux control and communication, broadband nonreciprocal emitters are desirable for enhancing the magnitude of heat flux and bandwidth of communication.

Nonreciprocal emission and absorption are predicted in systems with magneto-optical materials [35–38], Kerr nonlinearity [39], or time modulation [40]. Existing designs of nonreciprocal emitters typically rely on critical coupling in one resonance [35–37] or two resonances [41,42]. Accordingly, strong nonreciprocal emission is achieved only near one or two resonances, leading to a narrow bandwidth. To date, despite the importance of broadband nonreciprocal emission for energy harvesting, heat-flux control, and communication, a general strategy for achieving broadband nonreciprocal emission is elusive.

Here, we introduce a general approach for achieving broadband nonreciprocal emission by using a gradient epsilon-near-zero magneto-optical metamaterial. We elucidate the mechanism of nonreciprocal emission in a thin film using the temporal coupled-mode theory. We then numerically demonstrate broadband nonreciprocal emission in gradient doped semiconductors and magnetic Weyl semimetals with a gradient chemical potential. Our results can be useful for developing broadband nonreciprocal devices for energy conversion and thermal management.

II. NONRECIPROCAL EMISSION IN A SINGLE MAGNETO-OPTICAL LAYER

We begin by considering emission and absorption in the thin-film emitter shown in Fig. 1(a). The emitter consists of a magneto-optical film on top of a substrate. Without loss of generality, we consider 400 - nm-thick doped InSb film, and a substrate with relative permittivity $\epsilon_S = -2$. We consider TM polarization with emission angle θ. We first introduce the dielectric model of a doped semiconductor. For a doped semiconductor, in an external magnetic field, due to the free-carrier effect, the permittivity of the material is described by a nonsymmetric tensor [43]. With the magnetic field along the y axis, the relative permittivity tensor of doped InSb is

$$\overleftrightarrow{\epsilon} = \begin{bmatrix} \epsilon_\infty - \frac{\omega_p{}^2(\omega - i\Gamma)}{\omega[(\omega - i\Gamma)^2 - \omega_c{}^2]} & 0 & -\frac{i\omega_p{}^2\omega_c}{\omega[(\omega - i\Gamma)^2 - \omega_c{}^2]} \\ 0 & \epsilon_\infty - \frac{\omega_p{}^2}{\omega(\omega - i\Gamma)} & 0 \\ \frac{i\omega_p{}^2\omega_c}{\omega[(\omega - i\Gamma)^2 - \omega_c{}^2]} & 0 & \epsilon_\infty - \frac{\omega_p{}^2(\omega - i\Gamma)}{\omega[(\omega - i\Gamma)^2 - \omega_c{}^2]} \end{bmatrix},$$

where $\epsilon_\infty = 15.68$ is the high-frequency permittivity, $\omega_p = \sqrt{n_e e^2/(m^*\epsilon_0)}$ is the plasma frequency, Γ is the relaxation rate, and $\omega_c = eB/m^*$ is the cyclotron frequency. Here, n_e is the electron-doping concentration, e is the charge for a proton, m^* is the effective electron mass, and ϵ_0 is the vacuum permittivity. We consider a doping concentration of $n_e = 8 \times 10^{18}$ cm^{-3}. At such a doping concentration, the electron mobility is $\mu_n = 6730$ cm^{2}V^{-1} s^{-1} [44]; $m^* = 0.707\, m_e$, where m_e is the resting mass of the electron; and the relaxation rate

is $\Gamma = 3.658 \times 10^{12}$ rad s^{-1} from $\mu_n = e/(m^*\Gamma)$. The effective electron mass is calculated using a model [45,46] considering the nonparabolicity of the conduction band, $m^* = m_n[1 + (1/2)(3/\pi)^{2/3}(h^2/E_g m_n)n_e^{2/3}]^{1/2}$, where the band-gap energy is $E_g = 0.17$ eV at 300 K, $m_n = 0.014\ m_e$ is the electron effective mass at the bottom of the conduction band, and h is Planck's constant.

We calculate the emissivity and absorptivity of the structure in Fig. 1(a) using fluctuational electrodynamics [35, 47,48]. Without an external magnetic field, the emissivity and absorptivity are reciprocal, i.e., $\varepsilon(\theta, \lambda) = \alpha(\theta, \lambda)$, as shown in Fig. 1(b). In such a case, due to mirror symmetry with respect to the y-z plane, the emissivity is symmetric with respect to angle θ, that is, $\varepsilon(\theta, \lambda) = \varepsilon(-\theta, \lambda)$. The emission and absorption are due to the Berreman mode [14] at a wavelength of about 12.4 μm, where the diagonal component of permittivity (ϵ_{xx}) of the magneto-optical layer is near zero [Fig. 3(b)].

With an external magnetic field applied along the y axis, the emissivity and absorptivity change in opposite trends, as shown in Figs. 1(c) and 1(d). With a 3-T magnetic field, compared with the case without a magnetic field, the emissivity is greatly enhanced at angle $\theta > 0$ [Fig. 1(c)], and the absorptivity is greatly suppressed at angle $\theta > 0$ [Fig. 1(d)]. The enhancement of emissivity and the suppression of absorptivity at the same angle lead to strong breaking of the Kirchhoff's law of thermal radiation, i.e., $\varepsilon(\theta, \lambda) \neq \alpha(\theta, \lambda)$. As an example, at angle $\theta = 60^\circ$ and wavelength $\lambda = 12.35\ \mu$m, the emissivity and absorptivity are 0.908 and 0.112, respectively.

III. TEMPORAL COUPLED-MODE THEORY

We employ temporal coupled-mode theory to elucidate the mechanism of the strong nonreciprocal emission [49]. We consider an emission mode at resonance frequency ω_r. From temporal coupled-mode theory, the emissivity is

$$\varepsilon = \frac{4\gamma_i\gamma_e}{(\omega - \omega_r)^2 + (\gamma_i + \gamma_e)^2}, \tag{1}$$

where ω is the angular frequency. For the emission mode, the total modal decay rate is the sum of an intrinsic decay rate, γ_i, due to material loss and an external decay rate, γ_e, due to radiation. For a nearly lossless version of the emission mode, that is, when the intrinsic decay rate is near zero, the external decay rate exclusively defines the total modal decay rate.

We solve the dispersion relationship for the thin-film emitter structure shown in Fig. 1(a), for both the lossy case and the nearly lossless case with Γ set to zero. The dispersion relationship, $\omega(k_x)$, of the TM mode for the thin-film structure [50] is given by

$$i\tan(k_z d) = -\frac{\epsilon_{xx}k_z(k_{z,V} + (k_{z,S}/\epsilon_S))}{\epsilon_{xx}k_0^2 - k_x^2 + k_x\epsilon_{xz}(k_{z,V} - (k_{z,S}/\epsilon_S)) + k_{z,V}k_{z,S}(\epsilon_{xx}^2 + \epsilon_{xz}^2)/\epsilon_S}. \tag{2}$$

Here, k_x is the wavevector along the x axis; $k_0 = \omega/c$ is the wavevector in vacuum, where c is the velocity of light in vacuum; and $k_z = \sqrt{k_0^2(\epsilon_{xx} + (\epsilon_{xz}^2/\epsilon_{xx})) - k_x^2}$, $k_{z,V} = \sqrt{k_0^2 - k_x^2}$, and $k_{z,\,S} = \sqrt{\epsilon_S k_0^2 - k_x^2}$ denote the z component of the wavevector in the magneto-optical layer, vacuum, and the substrate, respectively. As the mode has loss, we solve the dispersion relationship with complex ω and real k_x [14]. The real part of the eigenfrequency represents the resonance frequency, ω_r, and the imaginary part of the eigenfrequency represents the total modal loss rate. Thus, the imaginary part of the eigenfrequency in the lossy case is $(\gamma_i + \gamma_e)$, and the imaginary part of the eigenfrequency in the nearly lossless case is the external decay rate, γ_e, from which the intrinsic decay rate, γ_i, can be obtained as the difference between the two.

Figure 2(a) shows the dispersion relationship of the thin-film emitter in varying magnetic fields. When there is no external magnetic field, the dispersion relationship is symmetric with respect to angle θ. In contrast, with an external magnetic field, the dispersion relationship becomes asymmetric with respect to θ, and thus, k_x. This can be understood from the fact that, with an external magnetic field, Eq. (2) has a dependence on k_x in the first order via $k_x\epsilon_{xz}(k_{z,V} - (k_{z,S}/\epsilon_S))$. The intrinsic decay rate, as shown in Fig. 2(b), shows a negligible dependence on the magnetic field and angle. The intrinsic decay rate is about $\Gamma/2$, which is consistent with fact that $\Gamma/2$ is the upper bound for the intrinsic decay rate [51] due to material loss.

In contrast, the external decay rate has a strong dependence on the magnetic field. As shown by Fig. 2(b), without a magnetic field, the external decay rate is much smaller than the intrinsic decay rate, leading to weak emissivity. As the magnetic field increases, at $\theta > 0$, the external decay rate increases, leading to its improved

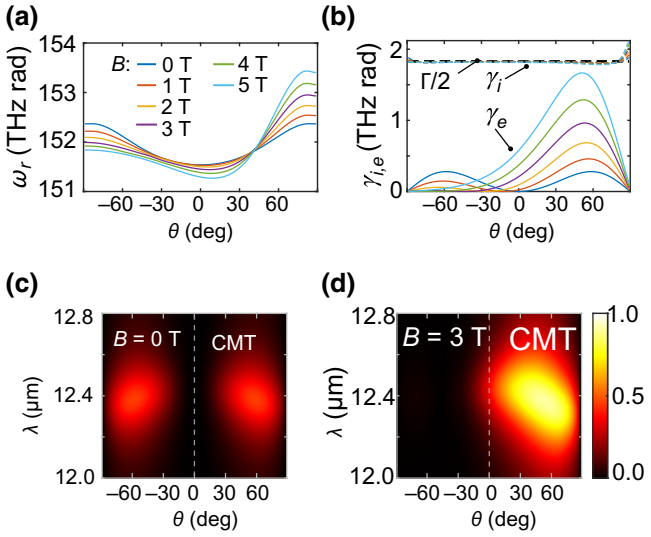

FIG. 2. Mechanism of nonreciprocal emission and absorption in one magneto-optical layer atop substrate. (a) Resonance frequency for the emission mode of the structure in Fig. 1(a) at varying angles θ and external magnetic fields B. (b) Intrinsic decay rate (dashed lines) and external decay rate (solid lines) of the emitter at varying angles and magnetic fields. (a),(b) Same color labeling. Black dashed line denotes $\Gamma/2$, where Γ is the relaxation rate. (c),(d) Emissivity, ε, predicted by temporal coupled-mode theory (CMT) when (c) there is no magnetic field and (d) when there is a 3-T magnetic field. Coupled-mode theory uses resonance frequency in (a) and decay rates in (b).

matching with the intrinsic decay rate. Due to the better matching between the two decay rates, enhanced emissivity is expected, which is consistent with Fig. 1(c). On the other hand, as the magnetic field increases, at $\theta < 0$, the contrast between the two decay rates further increases, suppressing emissivity [Fig. 1(c)]. Figures 2(c) and 2(d) show the emissivity predicted using Eq. (1) from temporal coupled-mode theory, with ω_r, γ_i, and γ_e calculated from the dispersion relationships without fitting parameters. The coupled-mode-theory results show excellent agreement with calculation based on fluctuational electrodynamics. Therefore, the opposite changes of the external decay rates at $\theta > 0$ and $\theta < 0$ in response to the magnetic field lead to strong asymmetry in the emissivity profile with respect to θ under a magnetic field, i.e., $\varepsilon(\omega, \theta) \neq \varepsilon(\omega, -\theta)$. Moreover, as $\alpha(\omega, \theta) = \varepsilon(\omega, -\theta)$ in specular emitters [35,52], such asymmetry in emissivity with respect to θ directly requires the breaking of Kirchhoff's law of thermal radiation, i.e., $\alpha(\omega, \theta) \neq \varepsilon(\omega, \theta)$. It is noteworthy that, when the magnetic field is sufficiently high, which is about 3 T in this case, raising the magnetic field further leads to an increase of the external decay rate at all angles, indicating the existence of an optimal magnetic field for breaking the reciprocity between emissivity and absorptivity.

IV. BROADBAND NONRECIPROCAL EMISSION IN GRADIENT EPSILON-NEAR-ZERO MAGNETO-OPTICAL METAMATERIAL

Building upon the thin-film emitter, we now introduce a general approach for achieving broadband nonreciprocal emission by using a gradient epsilon-near-zero (ENZ) magneto-optical metamaterial. The structure consists of a magneto-optical multilayer on top of a reflector, as shown in Fig. 3(a). In the multilayer, the ENZ condition for the magneto-optical material is met at progressively shorter wavelength as the depth increases. In such a way, as shown by Fig. 3(b), when the permittivity of one magneto-optical layer reaches near zero, the magneto-optical layer immediately underneath it has a negative permittivity, corresponding to the case of one magneto-optical layer (Fig. 1). Nonreciprocal emission due to the Berreman mode of each magneto-optical layer can then lead to a broadband nonreciprocal emission.

We numerically demonstrate broadband nonreciprocal emission using a gradient-doped semiconductor multilayer. To make the ENZ wavelength of the doped semiconductor decrease with depth, the doping level of the semiconductor is chosen to increase with depth. As an example, we consider a gradient-doped InSb multilayer, with electron-doping levels of 3.51×10^{18}, 4.21×10^{18}, 5.15×10^{18}, 6.36×10^{18}, and 8×10^{18} cm^{-3}, and with a 400 nm thickness for each layer. In this multilayer, when the permittivity of a specific layer is near zero, the layer immediately underneath is metallic with a relative permittivity of about -2, corresponding to the thin-film case in Fig. 1. The multilayer is backed by a reflector consisting of a 500-nm-thick undoped InSb dielectric spacer layer on top of Au. The spacer layer is used to enhance the nonreciprocal emission contributed by the bottom doped layer. Figures 3(c) and 3(d) show the emissivity and absorptivity of the multilayer, respectively, at 3-T magnetic field. There is a strong broadband emission at angle $\theta > 0$, corresponding to ENZ wavelengths of each individual doped layer. In contrast, the absorptivity is negligible for light incident at angle $\theta > 0$. Therefore, emissivity exceeds absorptivity over a broad band at $\theta > 0$, as shown in Fig. 3(e). In contrast, at angle $\theta < 0$, absorptivity exceeds emissivity. Finally, we note that a substantial difference between emission and absorption already exists at smaller magnetic fields. Figure 3(f) shows the difference between emissivity and absorptivity at $\theta = 50^\circ$ under varying magnetic fields. At $\theta = 50^\circ$, the difference between emissivity and absorptivity reaches 0.85 under a 3-T magnetic field, but is already significant, 0.40, under a 1-T magnetic field.

Our approach of using a gradient ENZ magneto-optical metamaterial for achieving broadband nonreciprocal emission is general. In the following, we show another broadband nonreciprocal emitter based on magnetic Weyl semimetals (MWSs) [53–56]. Magnetic Weyl

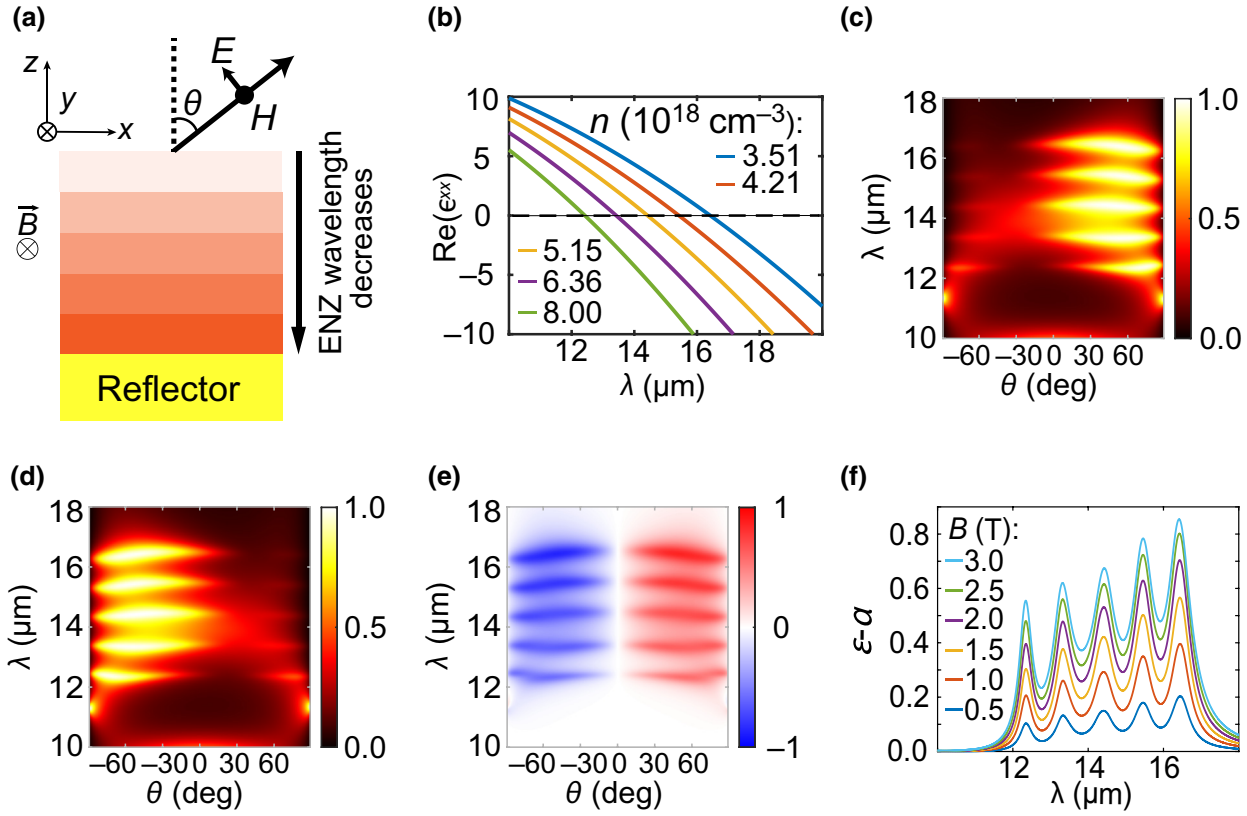

FIG. 3. Broadband nonreciprocal emitter based on a gradient epsilon-near-zero magneto-optical metamaterial. (a) Schematic of a gradient epsilon-near-zero magneto-optical metamaterial, on top of a reflector, where the ENZ wavelength of the magneto-optical layer decreases with depth. (b) Real part of permittivity (ϵ_{xx}) of doped InSb as a function of wavelength for varying doping levels, at a magnetic field of 3 T. In (c),(d), we consider a gradient-doped InSb multilayer, where the doping level increases with depth. Each doped InSb layer is 400 nm thick, with the corresponding doping level shown in (b). Reflector consists of 500-nm-thick undoped InSb atop Au. (c) Emissivity, ε; (d) absorptivity, α; and (e) difference between emissivity and absorptivity ($\varepsilon - \alpha$) of the gradient-doped InSb multilayer under a 3-T magnetic field. (f) Difference between emissivity and absorptivity of the muiltilayer at $\theta = 50^\circ$ under varying magnetic fields from 0.5 to 3 T.

semimetals can break the Lorentz reciprocity without an external magnetic field due to a strong anomalous Hall effect associated with enhanced Berry curvature near Weyl nodes. MWSs were recently used to theoretically design nonreciprocal emitters without an external magnetic field [36,37], although experiments of nonreciprocal emitters based on MWSs are yet to be demonstrated. We consider a multilayer emitter that consists of five MWS layers with a gradient chemical potential on top of Au, as shown in Fig. 4(a). In MWSs, the separation, 2**b**, between two Weyl nodes in the momentum space acts similarly to internal magnetization. When the momentum separation of Weyl nodes is aligned along the y axis, the relative permittivity tensor of the MWS is given by

$$\overleftrightarrow{\epsilon} = \begin{bmatrix} \epsilon_d & 0 & -i\epsilon_a \\ 0 & \epsilon_d & 0 \\ i\epsilon_a & 0 & \epsilon_d \end{bmatrix},$$

where $\epsilon_a = be^2/2\pi^2\hbar\omega$. The diagonal term, ϵ_d, has the form

$$\epsilon_d = \epsilon_b - \frac{ir_s g}{6\Omega_0}\Omega G\left(\frac{\Omega}{2}\right) - \frac{r_s g}{6\pi\Omega_0} \times \left\{\frac{4}{\Omega}\left[1 + \frac{\pi^2}{3}\left(\frac{k_B T}{E_F(T)}\right)^2\right] + 8\Omega\int_0^{\xi_c} \frac{G(\xi) - G(\Omega/2)}{\Omega^2 - 4\xi^2}\xi\, d\xi\right\}.$$

We follow Ref. [57] for the dielectric model of MWSs. Here, ϵ_b is the background permittivity; $r_s = e^2/4\pi\epsilon_0\hbar v_F$ is the effective fine-structure constant, where v_F is the Fermi velocity; $\Omega = \hbar(\omega + i\tau^{-1})/E_F$ is the normalized complex frequency, where τ is the scattering time; $E_F(T)$ is the chemical potential as a function of temperature T; $\Omega_0 = \hbar\omega/E_F$ is the normalized real frequency; and $G(E) = n(-E) - n(E)$, where $n(E) = 1/(e^{(E-E_F/k_BT)} + 1)$ is the Fermi-Dirac distribution and k_B

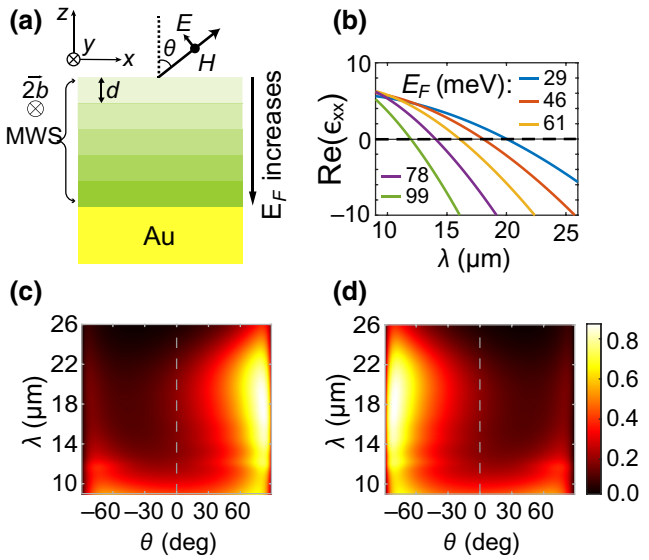

FIG. 4. Broadband nonreciprocal emitter based on MWS metamaterial. (a) Schematic of the emitter consisting of MWS layers with a gradient chemical potential atop Au. Each MWS layer has a thickness of 100 nm, and its chemical potential increases with depth. (b) Real part of permittivity tensor component, ϵ_{xx}, as a function of wavelength, λ, for varying chemical potentials at $T = 300$ K. (c) Emissivity, ε, and (d) absorptivity, α, of the MWS multilayer with gradient chemical potential.

is the Boltzmann constant. Following Refs. [57,58], we use $b = 8.5 \times 10^8\ \mathrm{m}^{-1}$, $\epsilon_b = 6.2$, $v_F = 0.83 \times 10^5\ \mathrm{m\,s}^{-1}$, $g = 2$, $\xi_c = 3$, and $\tau = 450$ fs. With nonzero momentum separation, the permittivity tensor of the MWS becomes asymmetric, breaking the Lorentz reciprocity. We consider a MWS multilayer structure, where each layer has a thickness of 100 nm, and its chemical potential increases with depth, as 29, 46, 61, 78, and 99 meV. As the chemical potential increases, the ENZ wavelength shifts to shorter wavelength, as shown in Fig. 4(b).

We show the calculated emissivity and absorptivity of the MWS multilayer in Figs. 4(c) and 4(d). The MWS multilayer with a gradient chemical potential shows a strong broadband emission at $\theta > 0$, but negligible absorption at the same angles, leading to broadband nonreciprocal emission and absorption. In contrast, the structure shows negligible emissivity at $\theta < 0$, but a strong broadband absorption at the same angles. The achieved spectral bandwidth of nonreciprocal emission is as large as 10 μm. The gradient chemical potential for the MWS may be achieved experimentally via doping [59–61] through controlling the types and concentrations of dopants.

We compare the broadband nonreciprocal emitters based on semiconductors and those based on magnetic Weyl semimetals. First, nonreciprocal emitters based on magnetic Weyl semimetals typically have a broader spectral bandwidth than those based on semiconductors. For the diagonal element of relative permittivity, when its real part is near zero, its imaginary part is about 0.01 and 1 for semiconductors and magnetic Weyl semimetals, respectively. As a larger imaginary part for the permittivity at the ENZ wavelength indicates larger intrinsic loss, an emitter based on magnetic Weyl semimetals has a broader bandwidth compared with that based on semiconductors. Second, the angular responses of the two emitters are different. The emitter based on magnetic Weyl semimetals has a narrower angular range than that based on semiconductors. Furthermore, the emission of the broadband nonreciprocal emitter based on magnetic Weyl semimetals peaks at a larger angle compared with that based on semiconductors. Finally, the broadband nonreciprocal emitter based on a semiconductor requires an external magnetic field. In contrast, the broadband nonreciprocal emitter based on a magnetic Weyl semimetal can function without an external magnetic field.

V. CONCLUSION AND DISCUSSION

We introduce a general approach to achieve broadband nonreciprocal emission and absorption by using a gradient epsilon-near-zero magneto-optical metamaterial. We use temporal coupled-mode theory to elucidate nonreciprocal emission and absorption in one magneto-optical layer. We then introduce a gradient epsilon-near-zero magneto-optical metamaterial as a general way for achieving broadband angle-selective nonreciprocal emission and absorption. We numerically demonstrate broadband nonreciprocal thermal emission in a gradient-doped semiconductor multilayer under a magnetic field, as well as in a magnetic Weyl semimetal multilayer with a gradient chemical potential without an external magnetic field. Our results are useful for designing broadband nonreciprocal emitters and absorbers for improving energy conversion, such as for solar cells and thermophotovoltaics; for harvesting outgoing thermal radiation; and for achieving nonreciprocal radiative thermal management and communication.

Finally, we provide a brief discussion on a few aspects towards the application of broadband nonreciprocal emitters, including working temperature, operating wavelength, and requirement for a magnetic field. We start by discussing the working temperature of broadband nonreciprocal emitters. In this work, we consider broadband nonreciprocal emitters at 300 K. First, we numerically demonstrate broadband nonreciprocal emitters based on InSb, due to its low electron effective mass, and thus, a large cyclotron frequency at a given magnetic field. InSb has a melting temperature of 800 K. We note that the material choice for achieving broadband nonreciprocal emission is quite general. Semiconductors [62], such as InAs, $InGa_{0.47}As_{0.53}$, GaAs, HgTe, PbTe, PbSe, and PbS, which have a low effective mass, can be used to

achieve similar effects. These semiconductors have melting temperatures near or higher than 1000 K. Second, certain magnetic Weyl semimetals have high Curie temperatures, such as Co_2MnGa at 690 K [53] and Co_2MnAl at 726 K [63]. Thus, broadband nonreciprocal emitters based on semiconductors and Weyl semimetals have the potential to work over a large temperature range. We note that, as the temperature changes, the optical properties of semiconductors and magnetic Weyl semimetals change, and thus, the design needs to be modified.

We discuss the operating wavelength of broadband nonreciprocal emitters. In our work, as numerical examples, we demonstrate broadband nonreciprocal emission at wavelengths of about 10–20 μm. Depending on the applications, the wavelength range for nonreciprocal emission and absorption needs to be tailored. For solar-energy harvesting and thermophotovoltaics, broadband nonreciprocal emission is required at wavelengths shorter than 10 μm. For harvesting outgoing radiation from an ambient atmosphere at 300 K to outer space, broadband nonreciprocal emission is needed at the mid-infrared region. Furthermore, for nonreciprocal heat-flux control and communication, the wavelength range of nonreciprocal emission depends on the temperature of the bodies and communication frequency. The wavelength range can be shifted to shorter (longer) wavelengths by increasing (reducing) the doping concentration of semiconductors and by increasing (reducing) the Fermi level of magnetic Weyl semimetals.

We further discuss the requirement for a magnetic field to achieve broadband nonreciprocal emission. For broadband nonreciprocal emitters based on semiconductors, the difference between emissivity and absorptivity reaches 0.85 under a 3-T magnetic field, but is already significant, 0.40, under a 1-T magnetic field. We note that, in a recent experiment [64], a magnetic field of similar magnitude (1.2 *T*) was generated using ferromagnets to achieve nonreciprocal absorption. Furthermore, we show that magnetic Weyl semimetals have the potential to support broadband nonreciprocal emission without using any magnetic field. Thus, our general strategy for achieving broadband nonreciprocal emission is useful and relevant for experiments and applications.

ACKNOWLEDGMENTS

This work is supported by the Charles E. Kaufman Foundation, a supporting organization of the Pittsburgh Foundation, and by start-up funding provided by the Pennsylvania State University.

[1] S. H. Fan, Thermal photonics and energy applications, Joule **1**, 264 (2017).

[2] W. Li and S. H. Fan, Nanophotonic control of thermal radiation for energy applications [Invited], Opt. Express **26**, 15995 (2018).

[3] D. G. Baranov, Y. Z. Xiao, I. A. Nechepurenko, A. Krasnok, A. Alu, and M. A. Kats, Nanophotonic engineering of far-field thermal emitters, Nat. Mater. **18**, 920 (2019).

[4] Y. Li, W. Li, T. C. Han, X. Zheng, J. X. Li, B. W. Li, S. H. Fan, and C. W. Qiu, Transforming heat transfer with thermal metamaterials and devices, Nat. Rev. Mater. **6**, 488 (2021).

[5] X. L. Liu, T. Tyler, T. Starr, A. F. Starr, N. M. Jokerst, and W. J. Padilla, Taming the Blackbody with Infrared Metamaterials as Selective Thermal Emitters, Phys. Rev. Lett. **107**, 045901 (2011).

[6] P. N. Dyachenko, S. Molesky, A. Y. Petrov, M. Stormer, T. Krekeler, S. Lang, M. Ritter, Z. Jacob, and M. Eich, Controlling thermal emission with refractory epsilon-near-zero metamaterials via topological transitions, Nat. Commun. **7**, 11809 (2016).

[7] M. Zhou, E. Khoram, D. J. Liu, B. Y. Liu, S. H. Fan, M. L. Povinelli, and Z. F. Yu, Self-focused thermal emission and holography realized by mesoscopic thermal emitters, ACS Photonics **8**, 497 (2021).

[8] A. C. Overvig, S. A. Mann, and A. Alu, Thermal Metasurfaces: Complete Emission Control by Combining Local and Nonlocal Light-Matter Interactions, Phys. Rev. X **11**, 021050 (2021).

[9] S. Y. Lin, J. G. Fleming, D. L. Hetherington, B. K. Smith, R. Biswas, K. M. Ho, M. M. Sigalas, W. Zubrzycki, S. R. Kurtz, and J. Bur, A three-dimensional photonic crystal operating at infrared wavelengths, Nature **394**, 251 (1998).

[10] D. L. C. Chan, M. Soljačić, and J. D. Joannopoulos, Thermal emission and design in 2D-periodic metallic photonic crystal slabs, Opt. Express **14**, 8785 (2006).

[11] T. Inoue, M. De Zoysa, T. Asano, and S. Noda, Realization of dynamic thermal emission control, Nat. Mater. **13**, 928 (2014).

[12] A. P. Raman, M. A. Anoma, L. Zhu, E. Rephaeli, and S. Fan, Passive radiative cooling below ambient air temperature under direct sunlight, Nature **515**, 540 (2014).

[13] J. Xu, J. Mandal, and A. P. Raman, Broadband directional control of thermal emission, Science **372**, 393 (2021).

[14] S. Vassant, J. P. Hugonin, F. Marquier, and J. J. Greffet, Berreman mode and epsilon near zero mode, Opt. Express **20**, 23971 (2012).

[15] I. Liberal and N. Engheta, Manipulating thermal emission with spatially static fluctuating fields in arbitrarily shaped epsilon-near-zero bodies, Proc. Natl. Acad. Sci. U. S. A. **115**, 2878 (2018).

[16] V. W. Brar, M. C. Sherrott, M. S. Jang, S. Kim, L. Kim, M. Choi, L. A. Sweatlock, and H. A. Atwater, Electronic modulation of infrared radiation in graphene plasmonic resonators, Nat. Commun. **6**, 7032 (2015).

[17] R.-J. Shiue, Y. Gao, C. Tan, C. Peng, J. Zheng, D. K. Efetov, Y. D. Kim, J. Hone, and D. Englund, Thermal radiation control from hot graphene electrons coupled to a photonic crystal nanocavity, Nat. Commun. **10**, 109 (2019).

[18] M. A. Kats, R. Blanchard, S. Y. Zhang, P. Genevet, C. H. Ko, S. Ramanathan, and F. Capasso, Vanadium Dioxide as a Natural Disordered Metamaterial: Perfect Thermal

Emission and Large Broadband Negative Differential Thermal Emittance, Phys. Rev. X **3**, 041004 (2013).
[19] A. Lenert, D. M. Bierman, Y. Nam, W. R. Chan, I. Celanovic, M. Soljacic, and E. N. Wang, A nanophotonic solar thermophotovoltaic device, Nat. Nanotechnol. **9**, 126 (2014).
[20] Z. Omair, G. Scranton, L. M. Pazos-Outón, T. P. Xiao, M. A. Steiner, V. Ganapati, P. F. Peterson, J. Holzrichter, H. Atwater, and E. Yablonovitch, Ultraefficient thermophotovoltaic power conversion by band-edge spectral filtering, Proc. Natl. Acad. Sci. U. S. A. **116**, 15356 (2019).
[21] D. J. Fan, T. Burger, S. McSherry, B. Lee, A. Lenert, and S. R. Forrest, Near-perfect photon utilization in an air-bridge thermophotovoltaic cell, Nature **586**, 237 (2020).
[22] M. L. Brongersma, Y. Cui, and S. Fan, Light management for photovoltaics using high-index nanostructures, Nat. Mater. **13**, 451 (2014).
[23] Z. Yu, A. Raman, and S. Fan, Fundamental limit of nanophotonic light trapping in solar cells, Proc. Natl. Acad. Sci. U. S. A. **107**, 17491 (2010).
[24] Y. Zhai, Y. G. Ma, S. N. David, D. L. Zhao, R. N. Lou, G. Tan, R. G. Yang, and X. B. Yin, Scalable-manufactured randomized glass-polymer hybrid metamaterial for daytime radiative cooling, Science **355**, 1062 (2017).
[25] G. Kirchhoff, Ueber das Verhältniss zwischen dem Emissionsvermögen und dem Absorptionsvermögen der Körper für Wärme und Licht, Ann. Phys. **185**, 275 (1860).
[26] M. Planck, *The Theory of Heat Radiation* (Forgotten Books, London, 2013).
[27] R. Siegel, *Thermal Radiation Heat Transfer*, 4th ed. (Taylor & Francis, London, 2001).
[28] H. Ries, Complete and reversible absorption of radiation, Appl. Phys. B **32**, 153 (1983).
[29] M. A. Green, Time-asymmetric photovoltaics, Nano Lett. **12**, 5985 (2012).
[30] Y. B. Park, B. Zhao, and S. H. Fan, Reaching the ultimate efficiency of solar energy harvesting with a nonreciprocal multijunction solar cell, Nano Lett. **22**, 448 (2022).
[31] S. Buddhiraju, P. Santhanam, and S. H. Fan, Thermodynamic limits of energy harvesting from outgoing thermal radiation, Proc. Natl. Acad. Sci. U. S. A. **115**, E3609 (2018).
[32] W. Li, S. Buddhiraju, and S. Fan, Thermodynamic limits for simultaneous energy harvesting from the hot sun and cold outer space, Light: Sci. Appl. **9**, 68 (2020).
[33] Z. Zhang and L. Zhu, Nonreciprocal Thermal Photonics for Energy Conversion and Radiative Heat Transfer, Phys. Rev. Appl. **18**, 027001 (2022).
[34] Y. Hadad, J. C. Soric, and A. Alu, Breaking temporal symmetries for emission and absorption, Proc. Natl. Acad. Sci. U. S. A. **113**, 3471 (2016).
[35] L. Zhu and S. Fan, Near-complete violation of detailed balance in thermal radiation, Phys. Rev. B **90**, 220301(R) (2014).
[36] B. Zhao, C. Guo, C. A. C. Garcia, P. Narang, and S. H. Fan, Axion-field-enabled nonreciprocal thermal radiation in Weyl semimetals, Nano Lett. **20**, 1923 (2020).
[37] Y. Tsurimaki, X. Qian, S. Pajovic, F. Han, M. D. Li, and G. Chen, Large nonreciprocal absorption and emission of radiation in type-I Weyl semimetals with time reversal symmetry breaking, Phys. Rev. B **101**, 165426 (2020).
[38] Z. M. Zhang, X. H. Wu, and C. J. Fu, Validity of Kirchhoff's law for semitransparent films made of anisotropic materials, J. Quant. Spectrosc. Radiat. Transfer **245**, 106904 (2020).
[39] C. Khandekar, R. Messina, and A. W. Rodriguez, Near-field refrigeration and tunable heat exchange through four-wave mixing, AIP Adv. **8**, 055029 (2018).
[40] S. Buddhiraju, W. Li, and S. H. Fan, Photonic Refrigeration from Time-Modulated Thermal Emission, Phys. Rev. Lett. **124**, 077402 (2020).
[41] J. Wu, F. Wu, and X. H. Wu, Strong dual-band nonreciprocal radiation based on a four-part periodic metal grating, Opt. Mater. **120**, 111476 (2021).
[42] J. Wu, F. Wu, T. C. Zhao, M. Antezza, and X. H. Wu, Dual-band nonreciprocal thermal radiation by coupling optical Tamm states in magnetophotonic multilayers, Int. J. Therm. Sci. **175**, 107457 (2022).
[43] K. Seeger, *Semiconductor Physics: An Introduction*. Advanced Texts in Physics, 9th ed. (Springer, Berlin, Heidelberg, 2004).
[44] E. Litwin-Staszewska, W. Szymańska, and R. Piotrzkowski, The electron mobility and thermoelectric power in InSb at atmospheric and hydrostatic pressures, Phys. Status Solidi B **106**, 551 (1981).
[45] P. Byszewski, J. Kołodziejczak, and S. Zukotyński, The thermoelectric power in InSb in the presence of an external magnetic field, Phys. Status Solidi B **3**, 1880 (1963).
[46] S. Law, R. Liu, and D. Wasserman, Doped semiconductors with band-edge plasma frequencies, J. Vac. Sci. Technol., B **32**, 052601 (2014).
[47] S. Rytov, Y. A. Kravtsov, and V. Tatarskii, *Principles of Statistical Radiophysics* (Springer, Berlin, 1989).
[48] D. Polder and M. Vanhove, Theory of radiative heat transfer between closely spaced bodies, Phys. Rev. B **4**, 3303 (1971).
[49] L. X. Zhu, S. Sandhu, C. Otey, S. H. Fan, M. B. Sinclair, and T. S. Luk, Temporal coupled mode theory for thermal emission from a single thermal emitter supporting either a single mode or an orthogonal set of modes, Appl. Phys. Lett. **102**, 103104 (2013).
[50] See the Supplemental Material at http://link.aps.org/supplemental/10.1103/PhysRevApplied.19.014013 for a derivation of the dispersion relationship of the thin-film emitter.
[51] A. Raman, W. Shin, and S. Fan, Upper Bound on the Modal Material Loss Rate in Plasmonic and Metamaterial Systems, Phys. Rev. Lett. **110**, 183901 (2013).
[52] C. Guo, B. Zhao, and S. Fan, Adjoint Kirchhoff's Law and General Symmetry Implications for All Thermal Emitters, Phys. Rev. X **12**, 021023 (2022).
[53] I. Belopolski, *et al.*, Discovery of topological Weyl fermion lines and drumhead surface states in a room temperature magnet, Science **365**, 1278 (2019).
[54] D. F. Liu, A. J. Liang, E. K. Liu, Q. N. Xu, Y. W. Li, C. Chen, D. Pei, W. J. Shi, S. K. Mo, P. Dudin, *et al.*, Magnetic Weyl semimetal phase in a Kagome crystal, Science **365**, 1282 (2019).
[55] N. Morali, R. Batabyal, P. K. Nag, E. K. Liu, Q. A. Xu, Y. Sun, B. H. Yan, C. Felser, N. Avraham, and H. Beidenkopf, Fermi-arc diversity on surface terminations of the magnetic Weyl semimetal $Co_3Sn_2S_2$, Science **365**, 1286 (2019).
[56] P. G. Li, J. Koo, W. Ning, J. G. Li, L. X. Miao, L. J. Min, Y. L. Zhu, Y. Wang, N. Alem, C. X. Liu, *et al.*, Giant room

temperature anomalous Hall effect and tunable topology in a ferromagnetic topological semimetal Co_2MnAl, Nat. Commun. **11**, 3476 (2020).

[57] C. Guo, B. Zhao, D. H. Huang, and S. H. Fan, Radiative thermal router based on tunable magnetic Weyl semimetals, ACS Photonics **7**, 3257 (2020).

[58] O. V. Kotov and Y. E. Lozovik, Giant tunable nonreciprocity of light in Weyl semimetals, Phys. Rev. B **98**, 195446 (2018).

[59] K. Halterman, M. Alidoust, and A. Zyuzin, Epsilon-near-zero response and tunable perfect absorption in Weyl semimetals, Phys. Rev. B **98**, 085109 (2018).

[60] E. Haubold, K. Koepernik, D. Efremov, S. Khim, A. Fedorov, Y. Kushnirenko, J. van den Brink, S. Wurmehl, B. Buchner, T. K. Kim, *et al.*, Experimental realization of type-II Weyl state in noncentrosymmetric $TaIrTe_4$, Phys. Rev. B **95**, 241108(R) (2017).

[61] M. Chinotti, A. Pal, W. J. Ren, C. Petrovic, and L. Degiorgi, Electrodynamic response of the type-II Weyl semimetal $YbMnBi_2$, Phys. Rev. B **94**, 245101 (2016).

[62] O. Madelung, *Semiconductors: Data Handbook*, 3rd ed. (Springer, Berlin, 2004).

[63] R. Y. Umetsu, K. Kobayashi, A. Fujita, R. Kainuma, and K. Ishida, Magnetic properties and stability of $L2(1)$ and $B2$ phases in the Co_2MnAl Heusler alloy, J. Appl. Phys. **103**, 07D718 (2008).

[64] K. J. Shayegan, B. Zhao, Y. Kim, S. H. Fan, and H. A. Atwater, Nonreciprocal infrared absorption via resonant magneto-optical coupling to InAs, Sci. Adv. **8**, eabm4308 (2022).